HHS Public Access

Author manuscript

Cancer Cell. Author manuscript; available in PMC 2018 June 12.

Published in final edited form as:

Cancer Cell. 2017 June 12; 31(6): 833–843.e5. doi:10.1016/j.ccell.2017.04.012.

Inhibition of B Cell Receptor Signaling by Ibrutinib in Primary Central Nervous System Lymphoma

Michail S. Lionakis[1,#], **Kieron Dunleavy**[2,#], **Mark Roschewski**[2], **Brigitte C. Widemann**[3], **John A. Butman**[4], **Roland Schmitz**[2], **Diane E. Cole**[3], **Christopher Melani**[2], **Christine S. Higham**[3], **Jigar V. Desai**[2], **Michele Ceribelli**[5], **Lu Chen**[5], **Craig J. Thomas**[2,5], **Richard F. Little**[6], **Juan Gea-Banacloche**[3], **Sucharita Bhaumik**[3], **Maryalice Stetler-Stevenson**[3], **Stefania Pittaluga**[3], **Elaine S. Jaffe**[3], **John Heiss**[3], **Nicole Lucas**[2], **Seth M. Steinberg**[3], **Louis M. Staudt**[2,*], and **Wyndham H. Wilson**[2,*]

[1]Laboratory of Clinical Infectious Diseases, National Institute of Allergy and Infectious Diseases, Bethesda, MD

[2]Lymphoid Malignancies Branch, Center for Cancer Research, National Cancer Institute

[3]Pediatric Oncology Branch, Cancer Research, National Cancer Institute

[4]Radiology and Imaging Sciences, Clinical Center, National Institutes of Health

[5]Division of Preclinical Innovation, National Center for Advancing Translational Sciences, National Institutes of Health

[6]Cancer Therapy Evaluation Program, National Cancer Institute

SUMMARY

Primary central nervous system lymphoma (PCNSL) harbors mutations that reinforce B cell receptor (BCR) signaling. Ibrutinib, a BTK inhibitor, targets BCR signaling and is particularly active in lymphomas with *BCR* and *MYD88* mutations. We performed a proof of concept phase Ib study of ibrutinib monotherapy followed by ibrutinib plus chemotherapy (DA-TEDDi-R). In 18 PCNSL patients, 94% showed tumor reductions with ibrutinib alone, including patients having PCNSL with *CD79B* and/or *MYD88* mutations, and 86% of evaluable patients achieved a

Corresponding authors: Lead contact: Wyndham H. Wilson (wilsonw@mail.nih.gov), Louis M. Staudt (lstaudt@mail.nih.gov), Lymphoid Malignancies Branch, National Cancer Institute, Building 10, Room 4N/115, 9000 Rockville Pike, Bethesda, MD 20892.
[#]Co-first authors;
[*]Co-corresponding authors.

Author Contributions

Conceptualization, M.S.L., B.C.W., L.M.S. and W.H.W.; Methodology, M.S.L., B.C.W., C.J.T., R.F.L., L.M.S. and W.H.W.; Validation, M.S.L., R.S., C.S.H., J.V.D., M.C., L.C., C.J.T., S.B., L.M.S., and W.H.W., Formal Analysis, C.J.T., S.M.S., L.M.S. and W.H.W; Investigation, M.S.L., K.D., M.R., B.C.W., J.A.B., R.S., D.E.C., C.M., C.S.H., J.V.D., M.C., L.C., C.J.T., J.G., S.B., M.S., S.P., E.S.J., J.H., N.L., L.M.S., and W.H.W.; Resources, M.S.L., K.D., M.R., B.C.W., J.A.B., R.S., D.E.C., C.M., C.S.H., J.V.D., M.C., L.C., C.J.T., J.G., S.B., M.S., S.P., E.S.J., J.H., N.L., L.M.S., and W.H.W; Data Curation, N.L., L.M.S. and W.H.W.; Writing-original draft, L.S.M. and W.H.W.; Writing-Review and Editing, M.S.L., K.D., M.R., B.C.W., J.A.B., R.S., D.E.C., C.M., C.S.H., J.V.D., M.C., L.C., C.J.T., J.G., S.B., M.S., S.P., E.S.J., J.H., N.L., S.M.S., L.M.S., and W.H.W.; Visualization, M.S.L., K.D., B.C.W, C.J.T., L.M.S., and W.H.W.; Supervision, L.M.S., and W.H.W.; Project Administration, K.D. and W.H.W.; Funding Acquisition, L.M.S. and W.H.W.

complete remission with DA-TEDDi-R. Increased aspergillosis was observed with ibrutinib monotherapy and DA-TEDDi-R. Aspergillosis was linked to BTK-dependent fungal immunity in a murine model. PCNSL is highly dependent on BCR signaling and ibrutinib appears to enhance the efficacy of chemotherapy.

Graphical Abstract

Primary CNS lymphoma (PCNSL) harbors mutations that reinforce B cell receptor signaling. In a phase 1b study, Lionakis et al. observe promising therapeutic effects of the BTK inhibitor ibrutinib in PCNSL but also increased aspergillosis, which they show to link to BTK-dependent fungal immunity in a mouse model.

Keywords

ibrutinib; B cell receptor signaling; primary CNS lymphoma; *Aspergillus fumigatus*; BTK; macrophage

INTRODUCTION

Primary central nervous system lymphoma (PCNSL), a subtype of diffuse large B cell lymphoma, has a cure rate below 40% with methotrexate-based regimens and is subject to late recurrences (Ambady et al., 2015; Rubenstein et al., 2013a). PCNSL tumors harbor mutations targeting the BCR subunit CD79B (*CD79B*) and the Toll-like receptor adaptor protein MYD88 (*MYD88*) (Braggio et al., 2015; Bruno et al., 2014; Chapuy et al., 2016; Hattori et al., 2016; Nakamura et al., 2016; Vater et al., 2015). These mutations potentiate chronic active BCR signaling and promote cell survival in activated B cell (ABC) DLBCL (Davis et al., 2010; Ngo et al., 2011; Wilson et al., 2015), suggesting that PCNSL tumors may be similarly addicted to BCR signaling. Ibrutinib, an inhibitor of Bruton's tyrosine kinase (BTK), blocks NF-κB activation downstream of BCR signaling and has significant clinical activity in relapsed/refractory ABC DLBCL, particularly in tumors harboring both a *CD79B* mutant isoform and a particular *MYD88* mutant isoform, L265P (Wilson et al., 2015). We hypothesized that ibrutinib would be highly active in PCNSL based on the high frequency of *CD79B* and/or *MYD88* L265P mutations in these tumors.

We were concerned that ibrutinib monotherapy would only produce short term remissions, since the median survival of patients with relapsed/refractory ABC DLBCL treated with ibrutinib monotherapy was 10.3 months (Wilson et al., 2015). Thus, we were interested in augmenting the efficacy of ibrutinib using chemotherapy agents capable of entering the central nervous system. Several active drugs are currently employed in standard treatment regimens for PCNSL and are potential choices for combination with ibrutinib (Rubenstein et al., 2013b). Not included among these is doxorubicin, which is pivotal for the curative treatment of systemic DLBCL but does not penetrate the blood-brain barrier (Anders et al., 2013; Wilson, 2013). An alternative liposomal formulation of doxorubicin overcomes this impediment and is a particularly promising drug to combine with ibrutinib for the treatment of PCNSL (Anders et al., 2013; Caraglia et al., 2006; Koukourakis et al., 2000; Lin et al., 2004; Siegal et al., 1995; Vail et al., 2004). The combination of ibrutinib with

chemotherapeutic agents is rational since ibrutinib treatment of ABC DLBCL cells inhibits the NF-κB pathway, which has been shown to antagonize the pro-apoptotic action of chemotherapeutic agents (Baldwin, 2001). Furthermore, ibrutinib has been shown to synergize with several chemotherapeutic agents in killing ABC DLBCL cells in vitro (Mathews Griner et al., 2014). Based on the above considerations, we investigated the potential of ibrutinib to produce clinical responses in PCNSL, both as a single agent and together with chemotherapy.

RESULTS

Ibrutinib and chemotherapy combinations in ABC DLBCL

To design a chemotherapy platform for PCNSL utilizing ibrutinib, we investigated whether various chemotherapeutic agents used to treat DLBCL or PCNSL would be superadditive (synergistic), additive or antagonistic in combination with ibrutinib in killing two cell line models of ABC DLBCL. We chose two cell lines that share genetic feature of PCNSL, namely the *MDY88* L265P mutation and mutations targeting the BCR subunits *CD79B* (TMD8) or *CD79A* (OCI-Ly10) (Braggio et al., 2015; Bruno et al., 2014; Chapuy et al., 2016; Hattori et al., 2016; Nakamura et al., 2016; Vater et al., 2015). We performed 10 × 10 dose titration experiments in which various ibrutinib concentrations were combined with various concentrations of four DNA-damaging chemotherapeutic agents, four anti-folate agents and one thymidylate synthase inhibitor (Figure 1A). Notably, the DNA-damaging agents – doxorubicin, etoposide, cytarabine and mitomycin C – were all super-additive/synergistic with ibrutinib in killing both TMD8 and OCI-Ly10 cells in vitro, as assessed by the DBSumNeg metric (See Methods; Figure 1A). This cooperativity likely reflects inhibition of NF-κB signaling by ibrutinib, since NF-κB is known to blunt the pro-apoptotic activity of chemotherapeutic agents (Baldwin, 2001) as previously noted (Mathews Griner et al., 2014). By contrast, all four anti-folate agents tested – methotrexate, pyrimethamine, pralatrexate and 4-aminofolic acid – showed little if any super-additive/synergistic action with ibrutinib (Figure 1A), but instead had higher values for a metric of antagonism, DBSumPos, than the DNA-damaging agents (Figure 1A). Interestingly, the thymidylate synthase inhibitor raltitrexed resembled the anti-folates in antagonizing ibrutinib action, suggesting that these effects may relate to the shared ability of these agents to interfere with DNA synthesis. As a class, the anti-folates were significantly more antagonistic ($p=3.5E-10$, t-test DBSumPos) and less synergistic ($p=9.4E-6$, t-test DBSumPos) with ibrutinib than the DNA-damaging agents (Figure 1A). The antagonism between ibrutinib and multiple structurally distinct anti-folates indicates that this is a class effect, and suggests that ibrutinib might not improve the efficacy of methotrexate-based regimens, which are the standard for the treatment of PCNSL. Because of the super-additivity/synergy between ibrutinib and DNA-damaging agents, we designed the DA-TEDDi-R regimen to include etoposide, cytarabine, and a liposomal formulation of doxorubicin (Doxil) that penetrates the central nervous system, unlike free doxorubicin (Figure 1B).

Clinical Characteristics and Treatment

Eighteen enrolled patients had a median (range) age of 66 (49–87) years, and performance status of 1 (1–3) (Table 1). Five patients were untreated, whereas 13 (72%) were relapsed (2)

or refractory (11) and received a median (range) of 2 (1–6) prior treatments. International Extranodal Lymphoma Study Group (IELSG) risk groups of 2–3 and 4–5 were present in 7 (39%) and 8 (44%) of patients, respectively (Ferreri et al., 2003).

Patients were treated at ibrutinib dose-levels of 560 mg (6), 700 mg (4) and 840 mg (8). Eighteen patients were treated on the ibrutinib "window" during which 2 patients developed grade 5 pulmonary/CNS aspergillosis (Table 2; Table S1). DA-TEDDi-R was administered to 16 patients over 74 cycles. The significant toxicities on DA-TEDDi-R were hematological and infectious (Table 2). Grade 4 neutropenia occurred on 53% of cycles, grade 4 thrombocytopenia on 30% of cycles and febrile neutropenia on 23% of cycles. Pulmonary infections occurred in 9 patients including 5 cases of aspergillosis, one case of *Pneumocystis jiroveci*, and 3 undetermined etiologies. Other infections included 2 cases of CNS aspergillosis, which also involved the lungs, and one case of enterocolitis. Other than infection, grade 3 and 4 non-hematological toxicities were infrequent (Table 2). Palmar plantar erythrodysesthesia (PPE), a common side effect of liposomal doxorubicin, was observed with grade 2 and 3 toxicity in 8 and 2 patients, respectively. Overall, the median (range) administered dose level of DA-TEDDi-R was 1 (−3 to 4) with 16% and 46% of cycles below and above dose level one, respectively.

Eight patients died; 3 from disease progression and 5 during treatment. Two patients died from *Aspergillus* infection during the ibrutinib window study, and one patient died of neutropenic sepsis on cycle 4 of DA-TEDDi-R (ibrutinib 840 mg dose level). Two deaths during treatment were not attributed to DA-TEDDi-R and included one retroperitoneal bleed/ventricular arrhythmia, and one non-hemorrhagic stroke. The retroperitoneal bleed occurred in a patient on enoxaparin for a deep vein thrombosis. On cycle 2 day 6, he developed an uncontrolled retroperitoneal bleed despite a platelet count of 139,000/μl that lead to hypotension, a ventricular arrhythmia and cardiac arrest. The stroke occurred on cycle 1 day 19 in a patient with a normal platelet count and 9 days after the last ibrutinib dose.

Based on the protocol definition, no toxicity was scored as a DLT and the maximum administered ibrutinib dose of 840 mg with DA-TEDDi-R was determined to be tolerated. Because the initial cases of aspergillosis were within the scope of clinically expected infections, they were not attributed to ibrutinib. However, based on the unexpectedly high number of aspergillosis cases, they were retrospectively attributed to ibrutinib but were not associated with ibrutinib plasma concentration.

Pharmacokinetics

Since the ability of ibrutinib to cross the blood-brain barrier had not been investigated, we performed detailed pharmacokinetics of ibrutinib and its primary metabolite, PCI-45227. The ibrutinib plasma and CSF maximum concentration (C_{max}) and area under the curve (AUC) did not increase proportionately over the 700 and 840 mg dose levels (Table 3). At 840 mg, the median (range) $AUC_{0–24\ nM•hr}$ in plasma and CSF were 977 (327–1562) and 7.7 (2.21–16.5), respectively with a CSF:plasma ratio of 0.78% (0.62–1.25), indicating low CSF penetration (Figure 2A; Table 3). When corrected for protein binding of 97.3%, the CSF:plasma ratio was 28.7% (23.2–446.6), indicating penetration of a significant fraction of

free drug into the CSF (Scheers et al., 2015). The time to maximum concentration (T_{max}) of approximately 2 hours was similar in the plasma and CSF and across dose levels, and the median plasma $T_{1/2}$ was 18.1 (4.1–31.2) hours. The time above the enzymatic IC_{50} (0.5 nM) in the CSF, a dynamic measure of drug exposure, showed a median (range) of 4 (0–24) hours at 840 mg, and was not proportional to dose. A comparison of ibrutinib plasma concentrations before and during DA-TEDDi-R did not show a significant pharmacokinetic interaction between ibrutinib and the chemotherapy drugs or decreased CSF penetration following treatment response (Table S2). The CSF penetration and kinetics of the ibrutinib metabolite PCI-45227 were similar to ibrutinib (Figure 2, Table S3). Thus, ibrutinib achieved significant CNS penetration at the doses administered and free drug concentrations within 4-fold of those in blood.

Pharmacokinetic analysis of liposomal doxorubicin was performed in 4 patients (#6, 7, 10, 11). The total doxorubicin plasma concentration time curves were characterized by sustained drug exposure and a median terminal half-life of 64.5 (range: 61.9–65.1) hours (Figure 2B). Doxorubicin was measurable in CSF in all patients, but CSF penetration was low with a median Cmax of 0.84 (range: 0.15–2.83) ng/mL (Figure 2B). Unexpectedly, the terminal half-life of doxorubicin in CSF could not be calculated due to persistently measurable concentrations throughout the sampling times.

Clinical outcome

Among 18 patients on the ibrutinib window study, all but one patient (17/18; 94%) had disease reductions and 83% (15/18; 95% Confidence Intervals (CI) 59–96%) achieved a partial response (Figure 3A, B) (Abrey et al., 2005). Two of these patients, both with refractory disease, normalized their research FDG-PET scans. Among 9 patients with CSF involvement, 2 (22%) became negative by flow cytometry on ibrutinib. The response rate to ibrutinib was similar in patients who were on pre-treatment steroids (91%; 10/11) compared to patients who received no pretreatment steroids (86%; 6/7), suggesting that stable doses of steroids did not enhance the activity of ibrutinib.

Sixteen patients began DA-TEDDi-R treatment. Two patients were not evaluable for response due to deaths that occurred prior to cycle 2 restaging that were unrelated to treatment. Of 14 evaluable patients, 86% (12/14; 95% CI 57–98%) achieved complete or complete response unconfirmed (CRu), one achieved a partial response and one had progressive disease (Figure 3C). Research FDG-PET scans were negative in all CR patients and in 6 of 9 CRu patients. Eight (57%) patients, including 5 with refractory disease, continue to be progression-free at a median (range) of 15.5 (8–27) months follow-up (Figure 3D). Considering all 13 patients with relapsed/refractory disease, the median progression-free survival based on Kaplan-Meier analysis from the on-study date to last follow-up is 15.3 months (95% CI: 1.3 months to undefined), while the overall survival median was not reached with 51.3% (95% CI: 21.4–74.9%) of patients alive at one year. Among the patients with relapsed or refractory disease, 6 progressed and/or died. Three patients progressed 142, 221 and 269 days after achieving CRu and one died. One CRu patient died of sepsis on treatment, one PR patient died with aspergillosis, and one patient progressed on DA-TEDDi-R and died.

CD79B and *MYD88* mutations in PCNSL

A previous evaluation of ibrutinib monotherapy in systemic ABC DLBCL revealed frequent responses in tumors bearing mutations targeting the *CD79B* ITAM signaling motif together with *MYD88* L265P (Wilson, 2013), prompting us to investigate the frequency of these mutations in PCNSL. First, we performed a meta-analysis of 6 published exome sequencing studies in PCNSL (Braggio et al., 2015; Bruno et al., 2014; Chapuy et al., 2016; Hattori et al., 2016; Nakamura et al., 2016; Vater et al., 2015). Overall, *MYD88* L265P mutations represented 90% of all mutations affecting the MYD88 TIR domain in PCNSL. *CD79B* ITAM and *MYD88* L265P mutations were reported in 56% and 53% of tumors, respectively, with 76% of tumors having one or both genetic events (Figure 4A). *CD79B* and *MYD88* L265P mutations were coincident in 37% of cases, which is significantly higher than observed systemic ABC DLBCL (10%)($p<0.0001$; Figure 4A) (Ngo et al., 2011).

Tumor specimens were available for *CD79B* and *MYD88* sequence analysis from 4 patients on the DA-TEDDi-R trial (Figure 4B). Two tumors only had *CD79B* mutations: one had the recurrent Y196C mutation targeting the first tyrosine in the ITAM motif while the other had a mutation in the splice acceptor site of *CD79B* exon 5, predicted to remove this same tyrosine from the encoded protein. One tumor had only *MYD88* L265P and another had both *CD79B* Y196C and *MYD88* L265P mutations. Each of these patients had a PR to ibrutinib monotherapy and achieved a CR with DA-TEDDi-R. Although the number of tumors available for analysis was limited, these data suggest that the response of PCNSL to ibrutinib does not depend on the presence of a *CD79B* or a *MYD88* mutation in an obligatory fashion based on the frequency of these mutations in other series (Figure 4A).

Aspergillus infections

Seven of 18 (39%) patients developed proven (3), probable (1) or possible (3) invasive aspergillosis (Figure 5A; Table 2; Table S1). Two patients who had been on dexamethasone for 2 and 4 weeks pre-treatment, respectively, for control of CNS swelling developed pulmonary and CNS aspergillosis during the ibrutinib window (Figure 5A, B, C). Despite anti-fungal treatment, both patients died from aspergillosis and autopsy showed *Aspergillus fumigatus* in their lungs and brain.

Five patients developed aspergillosis during DA-TEDDi-R treatment. Two treatment-naïve patients developed pulmonary symptoms at the end of cycle 4 and 5, respectively. Following anti-fungal treatment, the former patient died from progressive disease but with pulmonary and CNS aspergillosis, and the pulmonary abnormalities resolved in the latter patient. Due to increasing concern over aspergillosis, surveillance chest CT scans were instituted every cycle. During surveillance, pulmonary aspergillosis was detected in 2 patients after the first and second cycles. Following anti-fungal treatment, the pulmonary nodules in both patients resolved. A fifth patient developed pulmonary nodules and CNS aspergillosis on the first cycle of DA-TEDDi-R, which resolved on anti-fungal therapy. None of the patients had prolonged neutropenia on treatment.

To assess immune competency, we compared pretreatment CD4 and CD8 T cells in patients who did and did not develop aspergillosis and detected no significant difference: medians

(range) of 450 (98–749) and 176 (57–352) versus 580 (116–1584) and 216 (76–845), respectively. Aspergillosis occurred at all dose levels of ibrutinib, but was more common at the 840 mg level where 5 of 8 patients developed disease. However, there was no difference in the ibrutinib plasma C_{max} for patients who did and did not develop aspergillosis (median (range) 265 (144–536) and 277 (92–508) nM, respectively), indicating no association with drug concentration.

Model of aspergillosis in *Btk* knockout mice

To assess the role of BTK in *Aspergillus fumigatus* immune surveillance, we analyzed the outcome of invasive aspergillosis in *Btk* knockout ($Btk^{-/-}$) and wild-type ($Btk^{+/+}$) mice (Figure 5D). Mice were maintained under specific pathogen-free conditions. Eight-to-eleven week old $Btk^{+/+}$ (n = 20) and $Btk^{-/-}$ (n = 26) mice were infected with *Aspergillus fumigatus* via pharyngeal aspiration. Mouse survival was monitored for 14 days following infection. $Btk^{-/-}$ mice exhibited significantly greater mortality (27%) after *Aspergillus fumigatus* infection compared to $Btk^{+/+}$ mice (0%) ($p = 0.013$ by exact log-rank test), as well as greater weight loss (Figure 5E), and more severe lung tissue damage and fungal burden assessed by histology (Figure 5F), indicating a contribution of BTK to the innate immune control of *Aspergillus* infection.

Discussion

Ibrutinib alone showed clinical activity in 94% of patients with 83% of patients achieving partial remissions that were independent of prior treatment or ibrutinib dose level. The ibrutinib response rate we observed is significantly higher than the reported 37% response rate to ibrutinib monotherapy in relapsed/refractory systemic ABC DLBCL (Wilson et al., 2015). In that study, it was notable that tumors with *CD79B* mutations, and especially those with both *CD79B* and *MYD88* L265P mutations, had significantly higher response rates to ibrutinib, suggesting that tumors with these mutations may be hyper-addicted to BCR signaling. A meta-analysis of DNA sequencing studies in PCNSL revealed *CD79B* ITAM and *MYD88* L265P mutations in 56% and 53% of tumors, respectively, with over three quarters of cases having one or both of these genetic events. Moreover, the frequency of tumors with both *CD79B* and *MYD88* L265P mutations was over 3-fold higher in PCNSL than in systemic ABC DLBCL (Ngo et al., 2011). The genetic enrichment of PCNSL with mutations that augment BCR signaling may explain, in part, their high response rate to ibrutinib. Besides PCNSL, other extranodal DLBCLs with an ABC-like gene expression phenotype also have a high frequency of *CD79B* and *MYD88* L265P mutations, including primary testicular DLBCL, primary breast DLBCL and primary cutaneous DLBCL, suggesting that these cancers might also respond frequently to ibrutinib (Chapuy et al., 2016; Kraan et al., 2013; Kraan et al., 2014; Pham-Ledard et al., 2012; Taniguchi et al., 2016). Interestingly, one ibrutinib-responsive PCNSL tumor only had *MYD88* L265P, demonstrating that BCR signaling in PCNSL does not require a *CD79B* mutation and may instead be driven by self-antigen engagement of the BCR, as shown in systemic ABC DLBCL (Young et al., 2015). Indeed, PCNSL tumors are highly enriched for BCRs that utilize the autoreactive V_H4-34 immunoglobulin heavy chain variable region, which is present in 55% of cases (Fishman, 2007) compared to 30% of ABC DLBCL cases (Young et

al., 2015). Based on the high rate of response of PCNSL to ibrutinib together with this genetic evidence, we conclude that the vast majority of PCNSL tumors depend on chronic active BCR signaling.

DA-TEDDi-R produced complete remissions in 86% of patients, which includes 8 patients who are free of disease at a median of 15.5 (range, 8–27) months follow-up. When considering all 11 patients with refractory disease, defined as no response to the last administered chemotherapy regimen, the median progression-free survival was 11.2 (95% CI: 0.8-undefined) months. At present, refractory PCNSL patients have few effective treatment options and a median survival of around 2 months (Langner-Lemercier et al., 2016). Although the present results are based on a limited number of patients, the high CR rate of DA-TEDDi-R in refractory PCNSL suggests it may significantly improve the outcome of this disease. The efficacy of ibrutinib in PCNSL and the pivotal role of doxorubicin for the cure of systemic DLBCL suggest that both these agents play an important role in the outcome of DA-TEDDi-R (Wilson, 2013). Furthermore, the in vitro synergy between ibrutinib and the DNA damaging agents in this regimen (doxorubicin, etoposide and cytarabine) in killing ABC DLBCL cells may contribute to the activity of these agents in combination. Our finding of in vitro antagonism between ibrutinib and anti-folates such as methotrexate raises the possibility that ibrutinib may not be as effective with standard chemotherapy regimens for PCNSL. Nonetheless, because methotrexate is the core drug for standard PCSNL regimens, it will be important to assess the safety and efficacy of ibrutinib with these methotrexate-containing regimens.

We measured ibrutinib and liposomal doxorubicin pharmacokinetics in the CSF as a surrogate of intracranial free-drug concentration (Liu et al., 2006). When considering the maximum administered dose of ibrutinib had a median CSF penetration of 28.7% and clinical activity in almost all patients, the results indicate that ibrutinib effectively inhibits BTK in PCNSL tumors. In contrast, the CSF penetration of liposomal doxorubicin was low but unexpectedly had measurable concentrations during the entire treatment cycle, suggesting a depot effect in the CNS. The CSF concentration of liposomal doxorubicin, which was measured on the first cycle, underestimates overall exposure due to drug accumulation on subsequent treatment cycles and enhanced uptake by tumor. Indeed, based on human and murine intracerebral breast cancer studies, liposomal doxorubicin achieved from 7–17-fold higher concentrations in tumor compared to normal brain (Anders et al., 2013; Koukourakis et al., 2000).

The most frequent serious DA-TEDDi-R toxicities were hematological, and one patient died from neutropenic sepsis. Grade 4 neutropenia occurred on 53% of cycles, which is the intent of the dose-adjustment scheme. In addition, most of these patients were elderly and had received multiple prior regimens, which could have contributed to bone marrow suppression. PPE was the most common non-hematological toxicity and will be further assessed in subsequent studies. There were 4 deaths unrelated to the chemotherapy, including two patients who developed invasive aspergillosis during the ibrutinib monotherapy window. Indeed, the high incidence of aspergillosis (39%) on this trial was an unexpected finding that is potentially attributable to ibrutinib since it occurred during ibrutinib monotherapy in 2 of 7 patients. Invasive aspergillosis rarely occurs in the absence of prolonged neutropenia,

which did not occur in our patients (Lewis et al., 2013; Singh, 2005). While high-dose and extended steroids are associated with aspergillosis, this typically occurs in conjunction with other risk factors and is uncommon in PCNSL (Lewis et al., 2013; Lionakis and Kontoyiannis, 2003; Singh, 2005). The rapidity of aspergillosis infection and high frequency of CNS involvement is unusual, but remarkably similar to a recent report of 3 patients with relapsed chronic lymphocytic leukemia on glucocorticoids who developed CNS aspergillosis within 2 months of starting ibrutinib (Ruchlemer et al., 2016). Importantly, an infection control review confirmed our cases were not associated with an outbreak of aspergillosis at our institution.

These findings suggest ibrutinib impairs fungal immune surveillance, a deficit that may be exacerbated by co-administration of dexamethasone and/or chemotherapy. Indeed, we found that $Btk^{-/-}$ mice have a higher mortality during pulmonary aspergillosis, demonstrating a role for BTK in innate fungal immune surveillance. Mechanistically, macrophages provide the first line of defense against fungi (Figure 5G)(Dubourdeau et al., 2006; Leopold Wager and Wormley, 2014; Limper et al., 1997). Exposure of macrophage Toll-like receptors (TLRs) to fungal pathogens initiates downstream signaling, including activation of BTK, that promotes adaptive immune responses (Figure 5G) (Chignard et al., 2007; Herbst et al., 2015; Horwood et al., 2006; Kasperkovitz et al., 2010; Lionakis and Kontoyiannis, 2003; Ramaprakash et al., 2009; Ramirez-Ortiz et al., 2008). In animal models, macrophage TLR9 activation is required for immunity and inflammatory responses to *Aspergillus fumigatus* (Herbst et al., 2015). Notably, TLR9 signals through BTK and calcineurin, and inhibition of calcineurin by tacrolimus contributes to aspergillosis in organ transplant patients (Byrne et al., 2013; Herbst et al., 2015; Singh, 2005). BTK is also required for NF-κB-dependent M1 macrophage polarization, which mediates host immunity against fungal pathogens (Ni Gabhann et al., 2014). The frequent involvement of the CNS by aspergillosis in our series raise the possibility that ibrutinib may inhibit CNS macrophages (microglia) (Dagenais and Keller, 2009; Lionakis and Kontoyiannis, 2003). The differentiation and function of neutrophils, which destroy hyphae through several mechanisms, involve BTK as well (Fiedler et al., 2011). Macrophage and neutrophil functions are also impaired by glucocorticoids, which likely further increased the risk of aspergillosis in our patients (Lionakis and Kontoyiannis, 2003). These considerations suggest that inhibition of BTK by ibrutinib contributed to the high incidence of aspergillosis, perhaps in concert with glucocorticoids. However, genetic loss of BTK function in humans with X-linked agammaglobulinemia (XLA) is associated with *P. jirovecii* infection but not aspergillosis, raising the possibility that alternative ibrutinib-sensitive mechanisms may affect the risk of aspergillosis (Plebani et al., 2002). Besides BTK, ibrutinib inhibits two other TEC-family kinase, ITK and BMX. ITK inhibition enhances T_H1 skewing, which would be predicted to promote M1 macrophage function and aspergillosis control (Dubovsky et al., 2013). While BMX is reported to enhance TLR-4/MYD88 signaling and hence macrophage activation, the absence of immunodeficiency associated with BMX loss suggests BMX inhibition by ibrutinib may not affect *Aspergillus* control (Palmer et al., 2008).

The high response rate of ibrutinib and the durable remissions following DA-TEDDi-R in refractory patients suggest that this regimen may significantly improve outcomes in PCNSL. Further development of this regimen will evaluate the efficacy of aspergillosis prophylaxis

using voriconazole, which has proven effective in preventing the aspergillosis that occurs during immunosuppression of patients receiving organ transplants (Fishman, 2007). A dose escalation study will be required to investigate predicted pharmacokinetic interactions between voriconazole and ibrutinib and liposomal doxorubicin. While further studies are needed to establish the risk of aspergillosis with ibrutinib, particularly in patients on steroids, physicians should be aware of this potential complication.

STAR METHODS

CONTACT FOR REAGENT AND RESOURCE SHARING

Further information and requests for resources and reagents should be directed to and will be fulfilled by the Lead Contact, Wyndham H. Wilson (wilsonw@mail.nih.gov).

EXPERIMENTAL MODEL AND SUBJECT DETAILS

Human Subjects—Patients were enrolled between August 14, 2014 and March 31, 2016. Eligible patients had a PCNSL diagnosis, untreated or relapsed/refractory disease, age of at least 18 years, and adequate major organ function. Pathological diagnosis was confirmed by SP and/or ESJ at the NCI. Patients were excluded if they had prior exposure to a BTK inhibitor, EBV+ PCNSL, and/or were pregnant and/or breast-feeding. The patient characteristics are shown in Table 1. The study was approved by the Institutional Review Board, patients provided written informed consent, and is registered on ClinicalTrials.gov NCT02203526.

Cell Lines—Two cell lines that share genetic feature of PCNSL were employed. The TMD8 cell contains a *MDY88* L265P mutation and *CD79B* mutation, and the OCI-Ly10 cell line contains a *CD79A* mutation (Braggio et al., 2015; Bruno et al., 2014; Chapuy et al., 2016; Hattori et al., 2016; Nakamura et al., 2016; Vater et al., 2015).

Mice—Wild-type ($Btk^{+/+}$) C57BL/6 mice were purchased from Taconic Biosciences. *Btk* knockout ($Btk^{-/-}$) mice, generated as described previously (Khan et al., 1995) and backcrossed for over 10 generations onto the C57BL/6 background, were obtained from Dr. Wasif Khan (University of Miami). $Btk^{+/+}$ and $Btk^{-/-}$ mice were maintained under specific pathogen-free housing conditions, with regular dark/light cycles and were provided water and food *ad libitum*. For all experiments, sex-matched (weight: 22–26 grams for male mice, 18–24 grams for female mice) and age-matched (8–11 week-old) $Btk^{+/+}$ and $Btk^{-/-}$ mice were used. All mouse experiments were approved by the Animal Care and Use Committee of the National Institute of Allergy and Infectious Diseases (protocol LCID14E) and were performed in strict accordance with the recommendations in the Guide for the Care and Use of Laboratory Animals of the National Institutes of Health.

METHOD DETAILS

Human Subject Study Design—The primary study objective was to identify a tolerated dose of ibrutinib with dose-adjusted temozolomide, etoposide, liposomal doxorubicin, dexamethasone, and rituximab (DA-TEDDi-R) (Figure 1C). Secondary objectives included ibrutinib response in a 14-day window, and DA-TEDDi-R toxicity and response rate. Initial

evaluation included standard laboratory investigations, HIV serology, whole body computed tomography and FDG-PET scans, and brain MRI and FDG-PET scans, CSF analysis by cytology and flow cytometric immunophenotyping, and ophthalmologic evaluation. An Ommaya reservoir was placed for intraventricular cytarabine and to study the plasma and CSF pharmacokinetics of ibrutinib and liposomal doxorubicin. CNS tumor responses were scored per the International PCNSL workshop response criteria and centrally assessed by JAB (Abrey et al., 2005). Tumor reductions during ibrutinib were based on MRI T1 post-contrast images.

Human Subject Treatment—The study investigated ibrutinib dose levels of 560, 700, and 840 mg administered orally once daily with 3–6 patients per dose level and up to 12 patients at the final dose level. If 0 of 3 patients experienced dose-limiting toxicity (DLT), escalation proceeded to the next dose level. A dose level at which no more than 1 of 6 patients experience DLT was considered to be safe.

Patients received ibrutinib alone in a “window” on day -14 to day -1 (Figure 1C). Involved sites were evaluated within 48 hours of beginning and 24 hours after stopping ibrutinib with brain MRI and FDG-PET scans, whole body CT and FDG-PET scans and CSF cytology and flow cytometry. Among 11 patients were receiving pre-treatment dexamethasone for symptom control, the dose was not increased above the initial dose within 2 weeks of beginning ibrutinib and if possible the dose was decreased before beginning ibrutinib. Immediately following ibrutinib, patients began DA-TEDDi-R, administered on days 1–10 of each 21-day cycle for a maximum of 6 cycles (Figure 1C and Supplement Section I). Pegfilgrastim was administered on day 6. Patients in the first cohort did not receive ibrutinib on cycle 1 of DA-TEDDi-R, but received ibrutinib on subsequent cycles. Temozolomide and etoposide were dose-adjusted by 20% in the absence of a neutrophil nadir < 500/mm^3, based on twice weekly blood counts. If the neutrophil nadir was < 500 mm^3 on 3 neutrophil measurements or the platelet nadir was < 25,000/mm^3, the doses were decreased 20% from the previous cycle. Liposomal doxorubicin was dose-reduced based on occurrence of palmar-plantar erythrodysesthesia (PPE) (Supplement Section II). Patients received prophylactic sulfamethoxazole 800 mg/trimethoprim 160 mg three days per week. Patients received 6 cycles of DA-TEDDi-R with restaging after cycles 2 and 6, and during follow-up every 3 months year one, 4 months year 2, 6 months year 3 and yearly thereafter. Dose-limiting toxicity (DLT) was assessed on cycle one of treatment and defined as events attributed to DA-TEDDi-R that included absolute neutrophil < 500/mm^3 > 7 days and platelets < 25,000/mm^3 > 10 days, and grade 3 nausea/emesis or diarrhea despite supportive therapy. Any unexpected grade 3 or higher non-hematological toxicity apart from grade 3 arthralgia or fatigue was dose-limiting.

Dose-Adjusted TEDDi-R Dose Adjustments and Evaluation—Treatment is usually administered on an outpatient basis. All patients start etoposide and temozolomide at dose level 1 of etoposide 50 mg and temozolomide 100 mg. Doses are adjusted based on the ANC nadir from the previous cycle per the chart below.

Drugs	Dose adjustment based on previous cycle nadir (see 6.1)							
	−2	−1	*1	2	3	4	5	6
Temozolomide (mg/m^2/day)	80	90	*100	120	144	173	207	248
Etoposide (mg/m^2/day)	40	45	*50	60	72	86.4	103.7	124.4

*Starting dose for all patients

Dose-adjustment for each treatment cycle

- Applies to etoposide and temozolomide based on previous cycle ANC or platelet nadir.
- Measurement of ANC and platelet nadirs are based on twice weekly CBC only (3 days apart). Only use twice weekly CBC for dose-adjustment, even if additional CBC's are obtained.
- To dose-adjust, all patients must receive a twice weekly complete blood count:
  - If Nadir ANC ≥ 500/μl on all measurements: Increase doses one level from last cycle.
  - If Nadir ANC < 500/μl on 1 or 2 measurements: Same doses as last cycle.
  - If Nadir ANC < 500/μl ≥ 3 measurements OR if platelet nadir <25,000μL on ≥ 1 measurement: Decrease doses one level from last cycle or stay at same level if already at level -2.

Day one treatment decisions

- If ANC ≥ 1000/μl and platelets ≥ 75,000/μl on day 21, begin treatment.
- If ANC < 1000/μl or platelets < 75,000/μl on day 21, delay up to 1 week. G-CSF may be started for ANC < 1000/μl and stopped 24 hours before treatment. If counts still low after 1 week delay, adjust doses ↓ one level from last cycle.

Evaluation time points

- Radiographic studies: Brain MRI/Brain FDG-PET/Body CT/Body FDG-PET.
  - Baseline, Day -1 Window study; Day 20–21 of Cycle 2, 4, 6 of DA-TEDDi-R; Post-DA-TEDDi-R every 3 months x 1 years, every 4 months x 1 year, every 6 months x 1 year and then yearly thereafter.
- CSF Flow Cytometry
  - Baseline, Day -1 Window study; Day 20–21 of Cycle 2, 4, 6 of DA-TEDDi-R if previous measurements were positive for lymphoma.

Dose-Adjusted TEDDi-R Dose Modifications

Mucositis dose modifications

- If patient has Grade 4 mucositis in previous cycle, decrease one dose level.

Liposomal doxorubicin dose modifications

Palmar-plantar erythrodysesthesia syndrome (PPE)	**Dose Adjustment**
First occurrence of **Grade 1:** Minimal skin changes or dermatitis (e.g., erythema, edema, or hyperkeratosis) without pain	Give liposomal doxorubicin 45 mg/m^2 and stay on schedule. If toxicity resolves to Grade 0 at start of next cycle, then liposomal doxorubicin dose may be re-escalated to 50 mg/m^2 on the next cycle per discretion.
Subsequent occurrence (s) of **Grade 1**	Give liposomal doxorubicin 45 mg/m^2.
First occurrence of **Grade 2:** Skin changes (e.g., peeling, blisters, bleeding, edema, or hyperkeratosis) with pain; limiting instrumental ADL	Give liposomal doxorubicin 40 mg/m^2 and stay on schedule. Cycle may be delayed up to 2 weeks, per discretion. If toxicity resolves to Grade 1 at start of next cycle, then liposomal doxorubicin dose may be re-escalated, per discretion, to 45 mg/m^2 on next cycle.
Subsequent occurrence (s) of **Grade 2**	Delay one week. If at one week toxicity has improved to Grade 0–1, give liposomal doxorubicin 45 mg/m^2. If at one week toxicity persists at Grade 2 give liposomal doxorubicin 40 mg/m^2.
First occurrence of **Grade 3:** Severe skin changes (e.g., peeling, blisters, bleeding, edema, or hyperkeratosis) with pain; limiting self-care ADL	Delay one week. If at one week toxicity has improved to Grade 0–1 give liposomal doxorubicin 45 mg/m^2. If at one week toxicity has improved to Grade 2 give liposomal doxorubicin 40 mg/m^2. Cycle may be delayed another week, per discretion. If at one week toxicity persists at Grade 3 delay one more week and re-evaluate.
Subsequent occurrence of **Grade 3:** Severe skin changes (e.g., peeling, blisters, bleeding, edema, or hyperkeratosis) with pain; limiting self-care ADL	Delay one week and re-evaluate. If at one week toxicity has improved to Grade 0–1 give liposomal doxorubicin 45 mg/m^2. If at one week toxicity has improved to Grade 2 give liposomal doxorubicin 40 mg/m^2.

Pharmacokinetics—Ibrutinib concentrations were measured in the ventricular CSF and plasma during the ibrutinib window before day -14; post-dose on day -14 at 1, 2, 4, 6, 8, between 10 to 18, and 24 hours; before day -13 dose; between day -4 and day -1 just prior to the dose and 2 hours after the dose. Ibrutinib concentrations were also measured during DA-TEDDi-R on cycles 2 and 5, just before day 1 dose and after 2 hours post-dose on day 5. Ibrutinib and metabolite PCI-45227 concentrations in cerebrospinal fluid (CSF) and sodium heparin plasma were measured using validated liquid chromatography with tandem mass spectrometry (LC-MS/MS) method (de Vries et al., 2015). Quantification range for ibrutinib and PCI-45227 in CSF was 0.100 to 25.0 ng/mL. To reduce adsorption 0.2% TWEEN-80 was added to CSF samples upon collection. Quantification range for ibrutinib and PCI-45227 in sodium heparin plasma was 0.500 to 100 ng/mL. Extraction Procedure: The ibrutinib and PCI-45227 were extracted from either plasma or CSF by protein precipitation by adding DMSO, internal standards spike solution and acetonitrile. D5-ibrutinib and D5-PCI-45227 were used as internal standards for quantifying each analyte. The mixture was vortex mixed and supernatant was transferred to 96 well Deep well plate. The supernatant was diluted by addition of 10 mM ammonium carbonate in water. It was then vortex mixed and injected into LC-MS/MS. HPLC-MS/MS conditions: A reversed phase LC-MS/MS method with analytical phenyl-hexyl column and a gradient separation was used for analysis. The mobile phase consisted of 10 mM ammonium carbonate in water and acetonitrile. Triple quadrupole mass spectrometer was used in a positive mode with an electro ion spray source. The mass spectrometer was set to a multiple reaction monitoring

mode for detecting analytes and internal standards. The peak areas for analytes were measured. Concentration Determination: Analyte concentrations in either CSF or plasma samples were obtained from a calibration curve constructed by plotting peak area ratio of the analyte to internal standard versus concentration. Analyte concentrations in samples were calculated using linear regression. The final plasma or CSF plasma concentration were used to determine pharmacokinetic parameters of ibrutinib and PCI-45227. Study Samples: Study samples were received frozen on dry ice from clinical sites to the bioanalytical laboratory. Upon receipt, all samples were stored frozen at a nominal temperature of −70 °C until analysis. Any discrepancies with sample identification were resolved prior to analysis.

Liposomal doxorubicin pharmacokinetics were studied in 4 patients. Total doxorubicin concentration (liposome bound + protein bound + free) was quantified using a validated liquid chromatography/tandem mass spectrometry assay (lower limit of quantification plasma=0.29 ng/mL, and CSF=0.06 ng/mL). Samples were obtained until a median of 345 hours (range 72–477 hours) after liposomal doxorubicin administration. All patient samples were kept at −80 °C until analysis. The total doxorubicin concentration (liposome bound + protein bound + free) was quantified with a validated liquid chromatography/tandem mass spectrometry assay. Daunorubicin was used as an internal standard for plasma samples. 100 μL of plasma standards, quality control (QC), and patient samples were extracted with acetonitrile (1:1 v/v), vortexed (30 sec.), and centrifuged for 5 min. (20,000 × g). Supernatant was diluted 1:1 (v/v) with 0.1% formic acid and 20 μL was injected on a 50 × 2.1 mm, 2.6 μ Accucore column (Thermo Scientific) using a Shimadzu Prominence HPLC system with a column heater set at 40 °C. A liner gradient was run starting with 70% A (0.1% formic acid) and 30% B (methanol with 0.1% formic acid) ramping to 90% B over 5 min., then returning to initial conditions. CSF standard, QC, and patient samples were diluted 1:10 (v/v) with 4% formic acid, vortexed (30 sec.) and centrifuged for 5 min. (20,000 × g). 40μL of supernatant was injected on the column using the same conditions as plasma. Detection was done on an API5000 tandem mass spectrometer (Sciex) in positive mode, monitoring transitions from *m/z* 544.2→ 397.1 (Doxorubicin, retention time: 4.75 min.) and *m/z* 528.2→ 363.2 (internal standard, retention time: 5.35 min.) Results were analyzed using Analyst 1.4.2 software (Sciex). PK parameters were estimated using non-compartmental methods. Pharmacokinetic parameters were estimated using non-compartmental methods.

In vitro model of ibrutinib and chemotherapy cytotoxicity—Matrix drug titration experiments were conducted in accordance with previously published methods (Mathews Griner et al., 2014). Briefly, each drug was dry-spotted into 1536-well cyclo-olefin polymer (COP) black clear bottomed plates at predetermined concentration ranges via acoustic dispensing using an ATS-100 (EDC Biosystems). TMD8 or OCI-Ly10 cells were added directly at 500 cells per well in 5 μL of media as previously reported. Following a 48 h incubation at 37 C under 5% CO2 with a 95% humidity level CellTiter Glo luminescent cell viability assay reagent (3 μL/well) (Promega) was added and the plates were incubated for 15 minutes before image acquisition. Luciferase activity was measured on a ViewLux reader with a 10-s exposure (Perkin-Elmer). Relative luminescence units for each well were normalized to median values from DMSO (full viability) and bortezomib (full cell killing)

control wells. Data were visualized through a web-based interface (https://tripod.nih.gov/matrix-client) incorporating a tabular summation of several synergy/additivity/antagonism metrics including the Bliss independence model (Bliss, 1939). A surrogate of drug synergy is the dbSumNeg metric, which represents the sum of the negative deviations from the Bliss model of drug independence across all elements in each 10 × 10 drug titration matrix. A surrogate of drug antagonism is the dbSumPos metric, which represents the sum of the positive deviations from the Bliss model of drug independence across all elements in each 10 × 10 drug titration matrix.

Analysis of *CD79B* and *MYD88* mutations—Genomic DNAs from 4 formalin-fixed and paraffin-embedded (FFPE) biopsies were analyzed by Sanger DNA sequencing to identify mutations in the region of *CD79B* encoding the ITAM motif and the region of MYD88 encoding the L265 residue using the primers: MYD88-E5F, 5′-gcaagggcctgatgccagcatg-3′; MyD88-E5R, 5′-gatacacacacacccagggcctc-3′; CD79B-E4R, 5′-acaccagcagatagtggccactgac-3′; CD79B-E4F, 5′-gggggacactaacactctgatctcc-3′; CD79B-E5R, 5′-agggagcctgcacccaggtcatg-3′; CD79B-E5F, 5′-tgtggtcccggcctgagttccac-3′.

Mouse Model of Pulmonary Aspergillosis—*Btk* wild-type ($Btk^{+/+}$) and knockout ($Btk^{-/-}$) mice were inoculated with freshly harvested conidia of the *Aspergillus fumigatus* strain B-5233 suspended in 30 μl of 0.01% Tween-20/PBS via pharyngeal aspiration, as described previously (Rao et al., 2003). In brief, mice were anesthetized with isoflurane, were placed on a board, and their tongues were gently held in full extension. The 30 μl conidial suspension was then released onto the base of the tongue with a pipette. The mice were then maintained with their tongue in full extension until at least two breaths were taken to ensure aspiration of the conidial suspension into the lungs. Within a minute after inoculation, all mice were awake. Three independent infection experiments were performed, all in the morning, in a total of 20 $Btk^{+/+}$ and 26 $Btk^{-/-}$ mice. Mouse survival was monitored daily for 14 days following infection, calculated using the Kaplan-Meier method and two-sided p-values were determined by the exact log-rank test. Mouse weight was recorded before infection and at day 3 post-infection in three independent experiments in a total of 11 $Btk^{+/+}$ and 9 $Btk^{-/-}$ mice. Mouse weight loss was calculated at day 3 post-infection relative to the uninfected state. $Btk^{+/+}$ and $Btk^{-/-}$ mice inoculated with *Aspergillus fumigatus* were euthanized on day 4 post-infection and their lungs were removed, fixed with 10% formalin, and embedded in paraffin. Tissue sections were processed for hematoxylin and eosin (H&E) and Grocott-Gomori's methenamine silver stain (GMS) staining (Histoserv, Inc., Germantown, Maryland). Two independent infection experiments were performed in a total of 7 $Btk^{+/+}$ and 7 $Btk^{-/-}$ mice.

QUANTIFICATION AND STATISTICAL ANALYSIS

The phase I clinical trial used a 3+3 design to evaluate toxicity; 3 to 6 patients were to be evaluated in each dose level, and up to a total of 12 at the highest safe dose level. Overall survival (OS) and progression free survival (PFS) were determined from the on-study date until the date of death or progression; patients remaining alive had their follow-up censored on November 30, 2016. The probability of PFS or OS was determined using the Kaplan-Meier method. For analyses of the mouse data, survival was calculated using the Kaplan-

Meier method and two-sided p values were determined by the exact log-rank test. Statistical analyses were performed using SAS version 9.3 (SAS Institute, Cary, NC) or Prism. Mouse weight loss was analyzed using the two-tailed unpaired *t*-test with Prism 6.0 software (GraphPad Software, San Diego, CA).

Supplementary Material

Refer to Web version on PubMed Central for supplementary material.

Acknowledgments

This research was supported by the Intramural Research Program of the NIH, National Cancer Institute and National Institute of Allergy and Infectious Disease.

References

Abrey LE, Batchelor TT, Ferreri AJ, Gospodarowicz M, Pulczynski EJ, Zucca E, Smith JR, Korfel A, Soussain C, DeAngelis LM, et al. Report of an international workshop to standardize baseline evaluation and response criteria for primary CNS lymphoma. J Clin Oncol. 2005; 23:5034–5043. [PubMed: 15955902]

Ambady P, Holdhoff M, Bonekamp D, Wong F, Grossman SA. Late relapses in primary CNS lymphoma after complete remissions with high-dose methotrexate monotherapy. CNS Oncol. 2015; 4:393–398. [PubMed: 26507609]

Anders CK, Adamo B, Karginova O, Deal AM, Rawal S, Darr D, Schorzman A, Santos C, Bash R, Kafri T, et al. Pharmacokinetics and efficacy of PEGylated liposomal doxorubicin in an intracranial model of breast cancer. PLoS One. 2013; 8:e61359. [PubMed: 23650496]

Baldwin AS. Control of oncogenesis and cancer therapy resistance by the transcription factor NF-kappaB. J Clin Invest. 2001; 107:241–246. [PubMed: 11160144]

Bliss CI. The toxicity of poisons applied jointly. Annals of Applied Biology. 1939; 26:585–615.

Braggio E, Van Wier S, Ojha J, McPhail E, Asmann YW, Egan J, da Silva JA, Schiff D, Lopes MB, Decker PA, et al. Genome-Wide Analysis Uncovers Novel Recurrent Alterations in Primary Central Nervous System Lymphomas. Clin Cancer Res. 2015; 21:3986–3994. [PubMed: 25991819]

Bruno A, Boisselier B, Labreche K, Marie Y, Polivka M, Jouvet A, Adam C, Figarella-Branger D, Miquel C, Eimer S, et al. Mutational analysis of primary central nervous system lymphoma. Oncotarget. 2014; 5:5065–5075. [PubMed: 24970810]

Byrne JC, Ni Gabhann J, Stacey KB, Coffey BM, McCarthy E, Thomas W, Jefferies CA. Bruton's tyrosine kinase is required for apoptotic cell uptake via regulating the phosphorylation and localization of calreticulin. J Immunol. 2013; 190:5207–5215. [PubMed: 23596312]

Caraglia M, Addeo R, Costanzo R, Montella L, Faiola V, Marra M, Abbruzzese A, Palmieri G, Budillon A, Grillone F, et al. Phase II study of temozolomide plus pegylated liposomal doxorubicin in the treatment of brain metastases from solid tumours. Cancer Chemother Pharmacol. 2006; 57:34–39. [PubMed: 16010592]

Chapuy B, Roemer MG, Stewart C, Tan Y, Abo RP, Zhang L, Dunford AJ, Meredith DM, Thorner AR, Jordanova ES, et al. Targetable genetic features of primary testicular and primary central nervous system lymphomas. Blood. 2016; 127:869–881. [PubMed: 26702065]

Chignard M, Balloy V, Sallenave JM, Si-Tahar M. Role of Toll-like receptors in lung innate defense against invasive aspergillosis. Distinct impact in immunocompetent and immunocompromized hosts. Clin Immunol. 2007; 124:238–243. [PubMed: 17604224]

Dagenais TR, Keller NP. Pathogenesis of Aspergillus fumigatus in Invasive Aspergillosis. Clin Microbiol Rev. 2009; 22:447–465. [PubMed: 19597008]

Davis RE, Ngo VN, Lenz G, Tolar P, Young RM, Romesser PB, Kohlhammer H, Lamy L, Zhao H, Yang Y, et al. Chronic active B-cell-receptor signalling in diffuse large B-cell lymphoma. Nature. 2010; 463:88–92. [PubMed: 20054396]

de Vries R, Huang M, Bode N, Jejurkar P, Jong J, Sukbuntherng J, Sips L, Weng N, Timmerman P, Verhaeghe T. Bioanalysis of ibrutinib and its active metabolite in human plasma: selectivity issue, impact assessment and resolution. Bioanalysis. 2015; 7:2713–2724. [PubMed: 26507928]

Dubourdeau M, Athman R, Balloy V, Huerre M, Chignard M, Philpott DJ, Latge JP, Ibrahim-Granet O. Aspergillus fumigatus induces innate immune responses in alveolar macrophages through the MAPK pathway independently of TLR2 and TLR4. J Immunol. 2006; 177:3994–4001. [PubMed: 16951362]

Dubovsky JA, Beckwith KA, Natarajan G, Woyach JA, Jaglowski S, Zhong Y, Hessler JD, Liu TM, Chang BY, Larkin KM, et al. Ibrutinib is an irreversible molecular inhibitor of ITK driving a Th1-selective pressure in T lymphocytes. Blood. 2013; 122:2539–2549. [PubMed: 23886836]

Ferreri AJ, Blay JY, Reni M, Pasini F, Spina M, Ambrosetti A, Calderoni A, Rossi A, Vavassori V, Conconi A, et al. Prognostic scoring system for primary CNS lymphomas: the International Extranodal Lymphoma Study Group experience. J Clin Oncol. 2003; 21:266–272. [PubMed: 12525518]

Fiedler K, Sindrilaru A, Terszowski G, Kokai E, Feyerabend TB, Bullinger L, Rodewald HR, Brunner C. Neutrophil development and function critically depend on Bruton tyrosine kinase in a mouse model of X-linked agammaglobulinemia. Blood. 2011; 117:1329–1339. [PubMed: 21063022]

Fishman JA. Infection in solid-organ transplant recipients. N Engl J Med. 2007; 357:2601–2614. [PubMed: 18094380]

Hattori K, Sakata-Yanagimoto M, Okoshi Y, Goshima Y, Yanagimoto S, Nakamoto-Matsubara R, Sato T, Noguchi M, Takano S, Ishikawa E, et al. MYD88 (L265P) mutation is associated with an unfavourable outcome of primary central nervous system lymphoma. Br J Haematol. 2016

Herbst S, Shah A, Mazon Moya M, Marzola V, Jensen B, Reed A, Birrell MA, Saijo S, Mostowy S, Shaunak S, Armstrong-James D. Phagocytosis-dependent activation of a TLR9-BTK-calcineurin-NFAT pathway co-ordinates innate immunity to Aspergillus fumigatus. EMBO Mol Med. 2015; 7:240–258. [PubMed: 25637383]

Horwood NJ, Page TH, McDaid JP, Palmer CD, Campbell J, Mahon T, Brennan FM, Webster D, Foxwell BM. Bruton's tyrosine kinase is required for TLR2 and TLR4-induced TNF, but not IL-6, production. J Immunol. 2006; 176:3635–3641. [PubMed: 16517732]

Kasperkovitz PV, Cardenas ML, Vyas JM. TLR9 is actively recruited to Aspergillus fumigatus phagosomes and requires the N-terminal proteolytic cleavage domain for proper intracellular trafficking. J Immunol. 2010; 185:7614–7622. [PubMed: 21059889]

Koukourakis MI, Koukouraki S, Fezoulidis I, Kelekis N, Kyrias G, Archimandritis S, Karkavitsas N. High intratumoural accumulation of stealth liposomal doxorubicin (Caelyx) in glioblastomas and in metastatic brain tumours. Br J Cancer. 2000; 83:1281–1286. [PubMed: 11044350]

Kraan W, Horlings HM, van Keimpema M, Schilder-Tol EJ, Oud ME, Scheepstra C, Kluin PM, Kersten MJ, Spaargaren M, Pals ST. High prevalence of oncogenic MYD88 and CD79B mutations in diffuse large B-cell lymphomas presenting at immune-privileged sites. Blood Cancer J. 2013; 3:e139. [PubMed: 24013661]

Kraan W, van Keimpema M, Horlings HM, Schilder-Tol EJ, Oud ME, Noorduyn LA, Kluin PM, Kersten MJ, Spaargaren M, Pals ST. High prevalence of oncogenic MYD88 and CD79B mutations in primary testicular diffuse large B-cell lymphoma. Leukemia. 2014; 28:719–720. [PubMed: 24253023]

Langner-Lemercier S, Houillier C, Soussain C, Ghesquieres H, Chinot O, Taillandier L, Soubeyran P, Lamy T, Morschhauser F, Benouaich-Amiel A, et al. Primary CNS lymphoma at first relapse/progression: characteristics, management, and outcome of 256 patients from the French LOC network. Neuro Oncol. 2016; 18:1297–1303. [PubMed: 26951382]

Leopold Wager CM, Wormley FL Jr. Classical versus alternative macrophage activation: the Ying and the Yang in host defense against pulmonary fungal infections. Mucosal Immunol. 2014; 7:1023–1035. [PubMed: 25073676]

Lewis RE, Cahyame-Zuniga L, Leventakos K, Chamilos G, Ben-Ami R, Tamboli P, Tarrand J, Bodey GP, Luna M, Kontoyiannis DP. Epidemiology and sites of involvement of invasive fungal infections in patients with haematological malignancies: a 20-year autopsy study. Mycoses. 2013; 56:638–645. [PubMed: 23551865]

Limper AH, Hoyte JS, Standing JE. The role of alveolar macrophages in Pneumocystis carinii degradation and clearance from the lung. J Clin Invest. 1997; 99:2110–2117. [PubMed: 9151783]

Lin NU, Bellon JR, Winer EP. CNS metastases in breast cancer. J Clin Oncol. 2004; 22:3608–3617. [PubMed: 15337811]

Lionakis MS, Kontoyiannis DP. Glucocorticoids and invasive fungal infections. Lancet. 2003; 362:1828–1838. [PubMed: 14654323]

Liu X, Smith BJ, Chen C, Callegari E, Becker SL, Chen X, Cianfrogna J, Doran AC, Doran SD, Gibbs JP, et al. Evaluation of cerebrospinal fluid concentration and plasma free concentration as a surrogate measurement for brain free concentration. Drug Metab Dispos. 2006; 34:1443–1447. [PubMed: 16760229]

Mathews Griner LA, Guha R, Shinn P, Young RM, Keller JM, Liu D, Goldlust IS, Yasgar A, McKnight C, Boxer MB, et al. High-throughput combinatorial screening identifies drugs that cooperate with ibrutinib to kill activated B-cell-like diffuse large B-cell lymphoma cells. Proc Natl Acad Sci U S A. 2014; 111:2349–2354. [PubMed: 24469833]

Nakamura T, Tateishi K, Niwa T, Matsushita Y, Tamura K, Kinoshita M, Tanaka K, Fukushima S, Takami H, Arita H, et al. Recurrent mutations of CD79B and MYD88 are the hallmark of primary central nervous system lymphomas. Neuropathol Appl Neurobiol. 2016; 42:279–290. [PubMed: 26111727]

Ngo VN, Young RM, Schmitz R, Jhavar S, Xiao W, Lim KH, Kohlhammer H, Xu W, Yang Y, Zhao H, et al. Oncogenically active MYD88 mutations in human lymphoma. Nature. 2011; 470:115–119. [PubMed: 21179087]

Ni Gabhann J, Hams E, Smith S, Wynne C, Byrne JC, Brennan K, Spence S, Kissenpfennig A, Johnston JA, Fallon PG, Jefferies CA. Btk regulates macrophage polarization in response to lipopolysaccharide. PLoS One. 2014; 9:e85834. [PubMed: 24465735]

Palmer CD, Mutch BE, Workman S, McDaid JP, Horwood NJ, Foxwell BM. Bmx tyrosine kinase regulates TLR4-induced IL-6 production in human macrophages independently of p38 MAPK and NFkapp}B activity. Blood. 2008; 111:1781–1788. [PubMed: 18025155]

Pham-Ledard A, Cappellen D, Martinez F, Vergier B, Beylot-Barry M, Merlio JP. MYD88 somatic mutation is a genetic feature of primary cutaneous diffuse large B-cell lymphoma, leg type. J Invest Dermatol. 2012; 132:2118–2120. [PubMed: 22495176]

Plebani A, Soresina A, Rondelli R, Amato GM, Azzari C, Cardinale F, Cazzola G, Consolini R, De Mattia D, Dell'Erba G, et al. Clinical, immunological, and molecular analysis in a large cohort of patients with X-linked agammaglobulinemia: an Italian multicenter study. Clin Immunol. 2002; 104:221–230. [PubMed: 12217331]

Ramaprakash H, Ito T, Standiford TJ, Kunkel SL, Hogaboam CM. Toll-like receptor 9 modulates immune responses to Aspergillus fumigatus conidia in immunodeficient and allergic mice. Infect Immun. 2009; 77:108–119. [PubMed: 18936185]

Ramirez-Ortiz ZG, Specht CA, Wang JP, Lee CK, Bartholomeu DC, Gazzinelli RT, Levitz SM. Toll-like receptor 9-dependent immune activation by unmethylated CpG motifs in Aspergillus fumigatus DNA. Infect Immun. 2008; 76:2123–2129. [PubMed: 18332208]

Rao GV, Tinkle S, Weissman DN, Antonini JM, Kashon ML, Salmen R, Battelli LA, Willard PA, Hoover MD, Hubbs AF. Efficacy of a technique for exposing the mouse lung to particles aspirated from the pharynx. J Toxicol Environ Health A. 2003; 66:1441–1452. [PubMed: 12857634]

Rubenstein JL, Gupta NK, Mannis GN, Lamarre AK, Treseler P. How I treat CNS lymphomas. Blood. 2013a; 122:2318–2330. [PubMed: 23963042]

Rubenstein JL, Hsi ED, Johnson JL, Jung SH, Nakashima MO, Grant B, Cheson BD, Kaplan LD. Intensive chemotherapy and immunotherapy in patients with newly diagnosed primary CNS lymphoma: CALGB 50202 (Alliance 50202). J Clin Oncol. 2013b; 31:3061–3068. [PubMed: 23569323]

Ruchlemer R, Ben Ami R, Lachish T. Ibrutinib for Chronic Lymphocytic Leukemia New England. Journal of Medicine. 2016; 374:1593–1594.

Scheers E, Leclercq L, de Jong J, Bode N, Bockx M, Laenen A, Cuyckens F, Skee D, Murphy J, Sukbuntherng J, Mannens G. Absorption, metabolism, and excretion of oral (1)(4)C radiolabeled

ibrutinib: an open-label, phase I, single-dose study in healthy men. Drug Metab Dispos. 2015; 43:289–297. [PubMed: 25488930]

Siegal T, Horowitz A, Gabizon A. Doxorubicin encapsulated in sterically stabilized liposomes for the treatment of a brain tumor model: biodistribution and therapeutic efficacy. J Neurosurg. 1995; 83:1029–1037. [PubMed: 7490617]

Singh N. Infectious complications in organ transplant recipients with the use of calcineurin-inhibitor agent-based immunosuppressive regimens. Curr Opin Infect Dis. 2005; 18:342–345. [PubMed: 15985832]

Stadler N, Hasibeder A, Aranda Lopez P, Teschner D, Desuki A, Kriege O, Weber AN, Schulz C, Michel C, Hess G, Radsak MP. The Bruton tyrosine kinase inhibitor ibrutinib abrogates triggering receptor on myeloid cells 1 mediated neutrophil activation. Haematologica. 2017

Taniguchi K, Takata K, Chuang SS, Miyata-Takata T, Sato Y, Satou A, Hashimoto Y, Tamura M, Nagakita K, Ohnishi N, et al. Frequent MYD88 L265P and CD79B Mutations in Primary Breast Diffuse Large B-Cell Lymphoma. Am J Surg Pathol. 2016; 40:324–334. [PubMed: 26752547]

Vail DM, Amantea MA, Colbern GT, Martin FJ, Hilger RA, Working PK. Pegylated liposomal doxorubicin: proof of principle using preclinical animal models and pharmacokinetic studies. Semin Oncol. 2004; 31:16–35.

Vater I, Montesinos-Rongen M, Schlesner M, Haake A, Purschke F, Sprute R, Mettenmeyer N, Nazzal I, Nagel I, Gutwein J, et al. The mutational pattern of primary lymphoma of the central nervous system determined by whole-exome sequencing. Leukemia. 2015; 29:677–685. [PubMed: 25189415]

Wilson WH. Treatment strategies for aggressive lymphomas: what works? Hematology Am Soc Hematol Educ Program. 2013; 2013:584–590. [PubMed: 24319235]

Wilson WH, Young RM, Schmitz R, Yang Y, Pittaluga S, Wright G, Lih CJ, Williams PM, Shaffer AL, Gerecitano J, et al. Targeting B cell receptor signaling with ibrutinib in diffuse large B cell lymphoma. Nat Med. 2015; 21:922–926. [PubMed: 26193343]

Young RM, Wu T, Schmitz R, Dawood M, Xiao W, Phelan JD, Xu W, Menard L, Meffre E, Chan WC, et al. Survival of human lymphoma cells requires B-cell receptor engagement by self-antigens. Proc Natl Acad Sci U S A. 2015; 112:13447–13454. [PubMed: 26483459]

SIGNIFICANCE

This study provides clinical results of ibrutinib in primary central nervous system lymphoma (PCNSL) and demonstrates inhibition of B cell receptor signaling is lethal in most tumors. Pharmacokinetics showed clinically effective ibrutinib concentrations in the cerebral spinal fluid (CSF), a surrogate of intracerebral concentrations. Liposomal doxorubicin, essential for cure of aggressive B cell lymphomas, was incorporated into the treatment of PCNSL and pharmacokinetics is consistent with achieving effective intratumoral concentrations. Combining these agents in the DA-TEDDi-R regimen produced complete remissions in most patients. A high occurrence of invasive *Aspergillus fumigatus* was observed with ibrutinib. A murine model of aspergillosis in *Btk* knockout mice confirmed susceptibility to fungal infection, likely due to inhibition of macrophage innate immune surveillance.

Highlights

- Ibrutinib reduced tumor masses in 94% of patients with primary brain lymphoma.
- Chronic active B cell receptor signaling is a feature of primary brain lymphoma.
- Ibrutinib promotes fungal infections with *Aspergillus fumigatus.*
- TEDDi-R treatment produced durable remissions in refractory primary brain lymphoma.

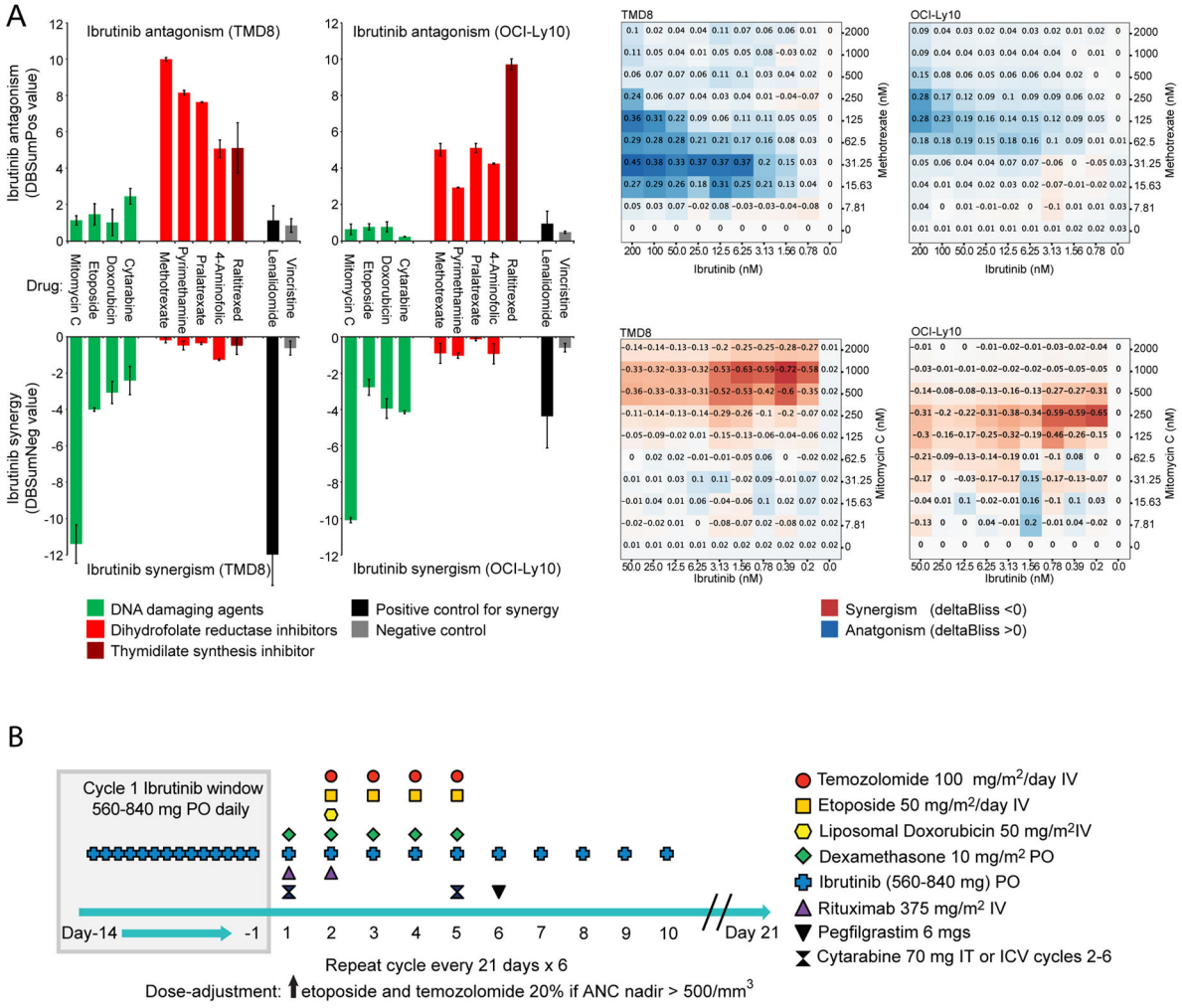

Figure 1. Ibrutinib-chemotherapy cytotoxicity models and DA-TEDDi-R Schema

(A) 10 x10 dose titration experiments were performed by combining a range of ibrutinib concentrations with a range of concentrations of the indicated agents in the TMD8 and OCI-Ly10 ABC DLBCL lines. The DBSumPos metric was used to summarize antagonism across the entire 10 × 10 block whereas the DBSumNeg metric was used to summarize drug synergy. For each selected ibrutinib combination pair, the average, plus or minus the SEM, is shown (2 biological replicates). Representative 10 × 10 dose-titration blocks are shown at the right with dose concentration combinations showing antagonism (blue) or synergy (red) highlighted. (**B**) DA-TEDDi-R treatment schema. Patients received ibrutinib alone in a 14-day 'window' (day -14 to -1) prior to cycle 1 of DA-TEDDi-R (temozolomide, etoposide, liposomal doxorubicin, dexamethasone, ibrutinib and rituximab) with intraventricular cytarabine. Abbreviations: IV- intravenous; PO-by mouth; IT-intrathecal; ICV-intracerebro-ventricular; ANC-absolute neutrophil count.

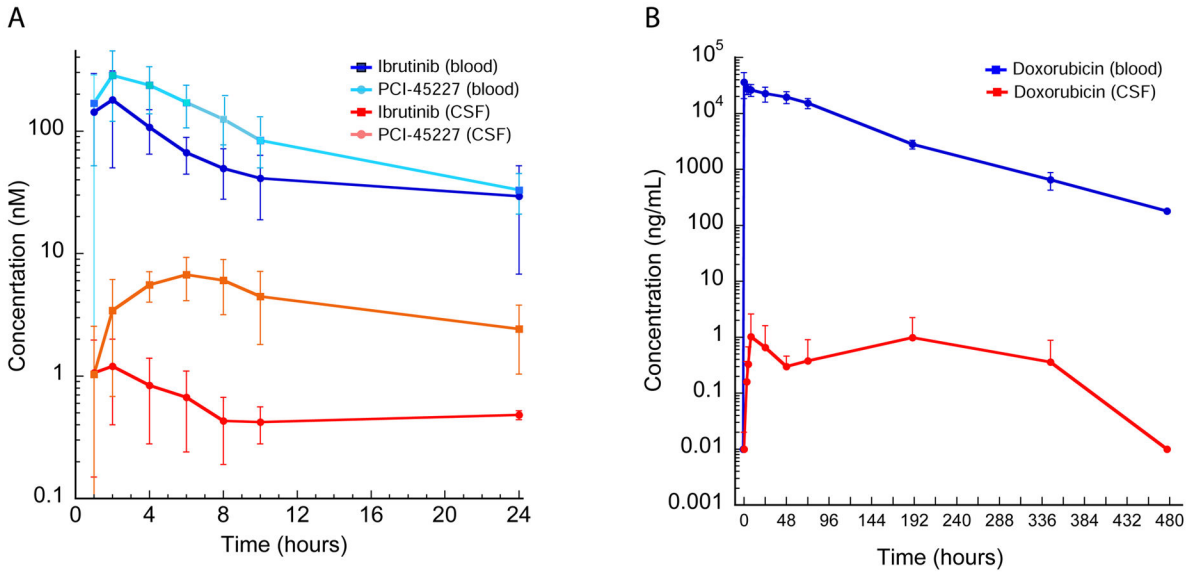

Figure 2. Pharmacokinetics of ibrutinib and metabolite (PCI-45227) and liposomal doxorubicin

A. Pharmacokinetics of ibrutinib and it metabolite PCI-45227 at the ibrutinib 840 mg dose level. Data represents the mean and standard deviation of patients 11–18 (8 patients). Ventricular CSF via ommaya reservoir and plasma were drawn during the ibrutinib window prior to day -14; post-dose on day -14 at 1, 2, 4, 6, 8, between 10 to 18, and at 24 hours and assayed for ibrutinib and PCI-45227 as indicated. **B.** Pharmacokinetics of liposomal doxorubicin in 4 patients. Data represent mean and standard deviation of total doxorubicin concentration (liposome bound + protein bound + free) in plasma and CSF. The mean Cmax in plasma and CSF were 41.4 (range: 23-2–61.5) and 0.61 (range: 0.15–2.83) ng/mL, respectively.

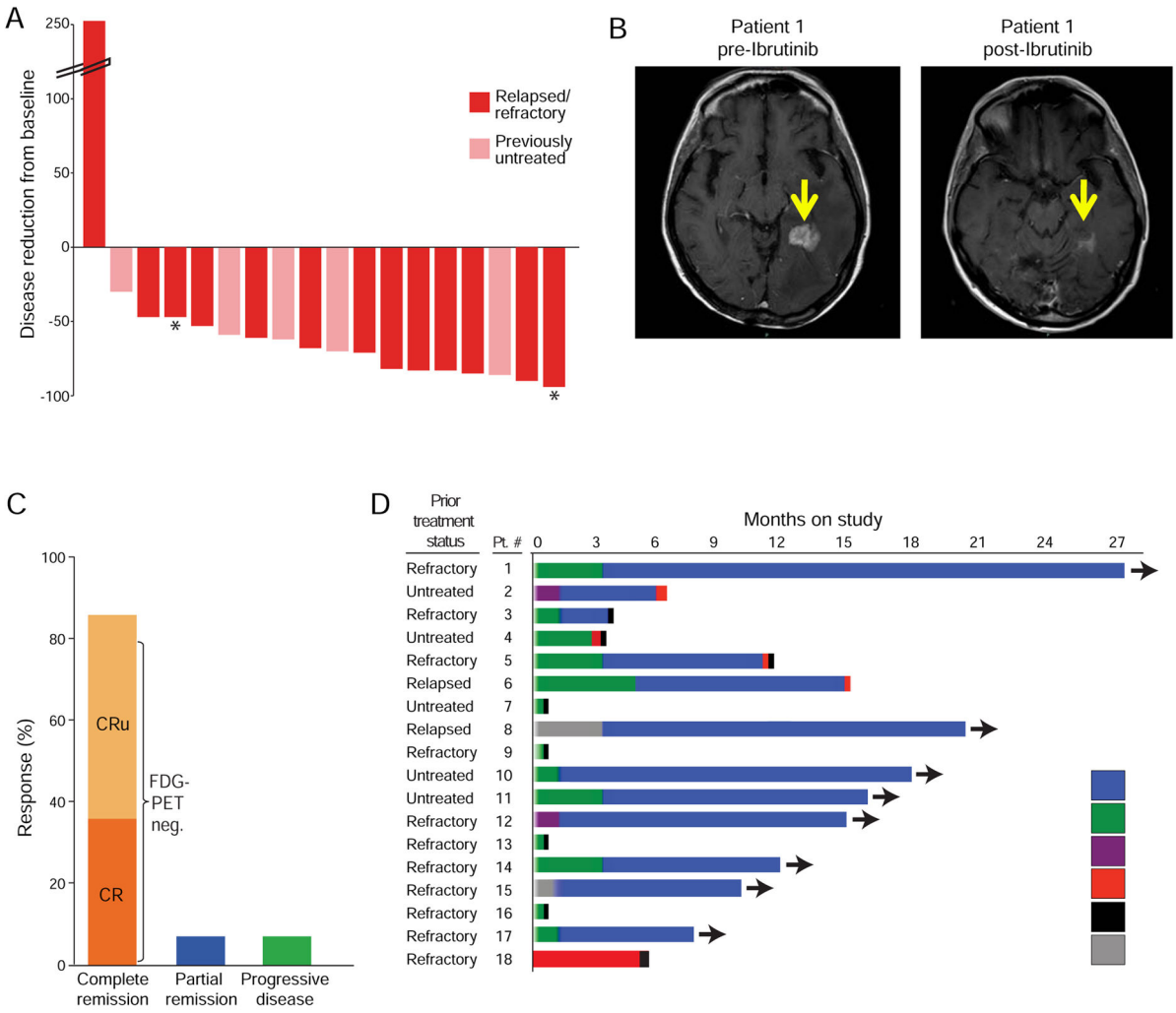

Figure 3. Clinical outcome of ibrutinib and DA-TEDDi-R treatment

A. Waterfall plot of maximum change from baseline of the product of the lesions for subjects with evaluable tumors on ibrutinib alone administered during the 'window' from day -14 to day -1 before initiation of DA-TEDDi-R (n=18). Two patients (*) with CSF and intraocular disease were assessed using quantitative estimates of tumor reductions. **B.** Representative brain MRI image before and after ibrutinib monotherapy in PCNSL patient 1. **C.** Best overall response rate achieved during DA-TEDDi-R therapy (n=16) and proportion of CR/CRu responses based on the International PCNSL workshop response criteria. The proportion of patients with negative research FDG-PET is shown. **D.** Swim lane plot of treatment duration and response for all patients on study (n=18). Prior treatment history is indicated by untreated, relapsed or refractory. Relapsed patients recurred following a complete response to prior treatment and refractory patients did not respond to prior chemotherapy. Abbreviations: CR-complete response; CRu-complete response unconfirmed; PR-partial response; PD-progressive disease; SD-stable disease; NE-not evaluable; FDG-PET-fluorodeoxy-glucose-positron emission tomography.

A

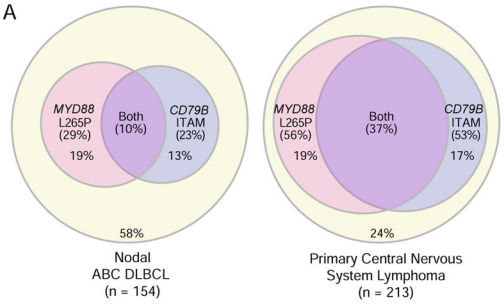

B

Pt. #	*CD79B* AA change	*MYD88* AA change	Ibrutinib response	DA-TEDDi-R response
1	Y196C	WT	PR	CR
5	splice acceptor (Y196 deletion)	WT	PR	CR
6	WT	L265P	PR	CR
11	Y196C	L265P	PR	CR

Figure 4. *CD79B* and *MYD88* mutations

A. Meta-analysis of the prevelance of *CD79B* ITAM and *MYD88* L265P mutations in 6 published PCNSL studies, compared with systemic ABC DLBCL. **B.** *CD79B* and *MYD88* sequence analysis of 4 patients on study based on accessions NP_000617 and NP_002459, respectively. The *CD79B* splice acceptor mutation in patient 5 involves exon 5, which encodes the Y196 residue of the ITAM motif and thus would be predicted to disrupt ITAM function.

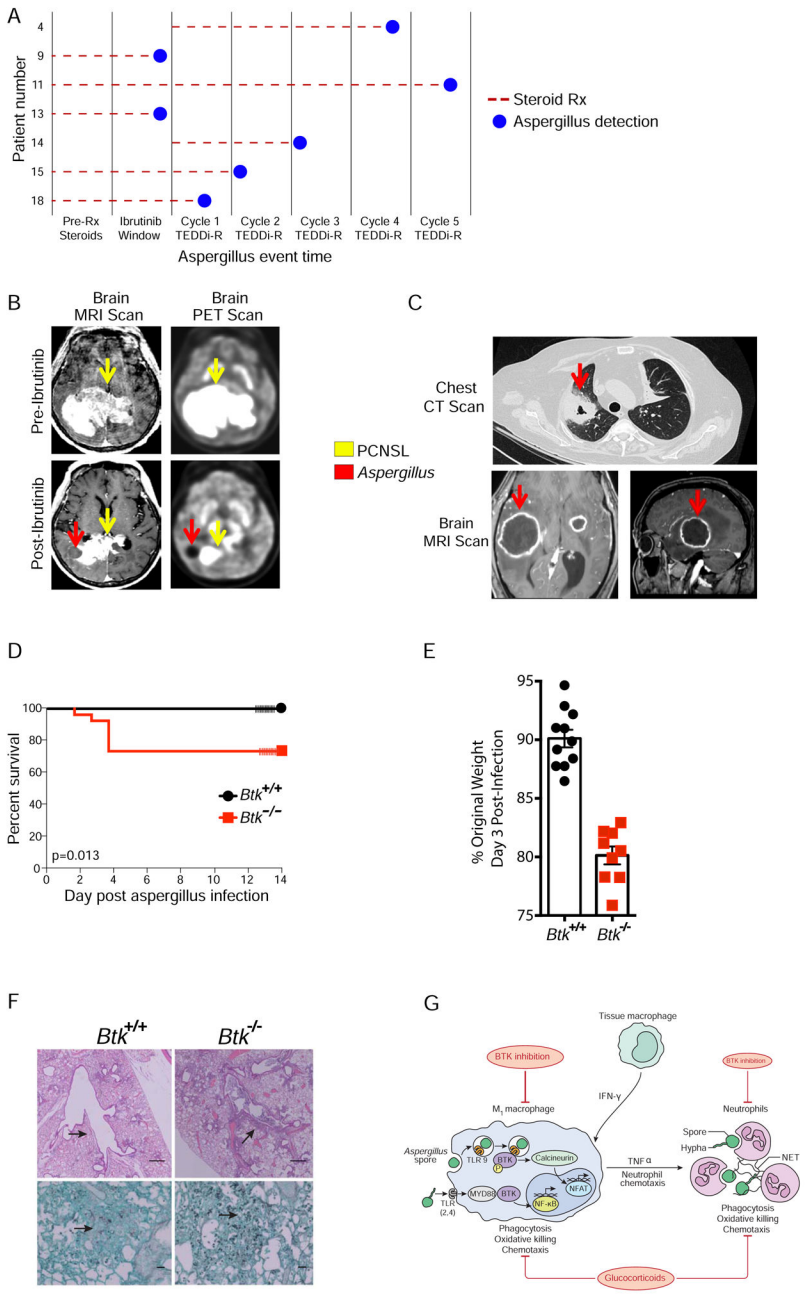

Figure 5. Association of *Aspergillus* with ibrutinib

A. *Aspergillus* event time and dexamethasone exposure. Seven patients developed aspergillosis of which 2 occurred on ibrutinib alone and 5 occurred during DA-TEDDi-R treatment. Five patients were receiving pre-treatment dexamethasone for control of brain edema. The patient numbers correspond to the swim lane numbers in Figure 3D. **B.** Brain MRI scans of *Aspergillus* infection in patient 9. MRI T1 post-contrast brain image pre-ibrutinib shows enhancing tumor and 13-days post-ibrutinib institution shows new *Aspergillus* abscesses and marked reduction in tumor enhancement. FDG-PET scans pre-ibrutinib shows metabolically active tumor and 13-days post-ibrutinib institution shows new

metabolically inactive *Aspergillus* abscesses and marked reduction in metabolically active tumor. **C.** Chest CT and brain MRI scans of *Aspergillus* infection in patient 13. Thirteen days post-ibrutinib, chest CT shows new cavitary *Aspergillus* abscess that was not present pre-ibrutinb. MRI T1 post-contrast brain images show new ring enhancing *A*spergillus abscesses that were not present pre-ibrutinib. **D.** Survival in murine model of *Aspergillus* infection in $Btk^{-/-}$ and $Btk^{+/+}$ mice. At 14-days of observation after pharyngeal aspiration of *Aspergillus fumigatus,* 7/26 $Btk^{-/-}$ mice exhibited mortality compared to 0/20 $Btk^{+/+}$ mice ($p = 0.013$; log-rank test) in 3 independent experiments. **E.** Weight loss in murine model of *Aspergillus fumigatus* at day 3 post-infection shown with standard error of the mean bars ($n = 9–11$) ($p< 0.0001$; unpaired *t*-test). **F.** Histology of representative lung sections from murine model of A*spergillus fumigatus* infection at day 4 post-infection ($n = 7$ $Btk^{-/-}$ and wild-type mice). Hematoxylin and eosin stain mages in upper panels (scale bars, 500 μm). Note more extensive peribronchial mononuclear cell and neutrophil inflammation with focal interstitial pneumonia and large airway mucous plugs in $Btk^{-/-}$ compared to $Btk^{+/+}$ mice lung as pointed out by arrows. Grocott-Gomori's methenamine silver stain (GMS) images in lower panels demonstrate more extensive *Aspergillus fumigatus* conidia in $Btk^{-/-}$ compared to $Btk^{+/+}$ mice as pointed out by arrows. **G.** Model of BTK and macrophage innate immunity to *Aspergillus*. Pulmonary macrophages are the first line of defense against inhaled *Aspergillus*. Toll-like receptors (TLRs) initiate signaling and the production of inflammatory cytokines on exposure to fungal conidia spores and hyphae. TLR2 and TLR4 are membrane bound and initiate signaling through BTK, which promotes the nuclear translocation of NF-κB (Horwood et al., 2006). Phagocytosis of *Aspergillus fumigatus* conidia induces TLR9 recruitment to the phagosome and through BTK, leads to activation of phospholipase Cγ and calcineurin-mediated NFAT nuclear translocation (Herbst et al., 2015). NF-κB acts in synergy with NFAT to produce TNFα that results in neutrophil recruitment. Neutrophils are chemotactically attracted to affected areas by TNFα and chemokines, and destroy fungal hyphae through oxidative and non-oxidative killing (Lionakis and Kontoyiannis, 2003). BTK can also affect the myeloid compartment, where it has a role in the differentiation and function of neutrophils (Fiedler et al., 2011; Stadler et al., 2017). Additionally, glucocorticoids impair the phagocytic, oxidative and chemotactic function of both macrophages and neutrophils, and are a risk factor for invasive aspergillosis infection (Lionakis and Kontoyiannis, 2003).

Table 1

Patient Characteristics

Characteristics	Number	Percent
Total Enrolled	18	100
Age Median (Range)	66 (49–87) years	
Male sex	11	61
ECOG Performance Status		
1	13	72
2	3	17
3	2	11
Histology: Large B-cell lymphoma (PCNSL)	18	100
Untreated PCNSL	5	28
Previously treated PCNSL	13	72
Median (range) regimens	2 (1–6)	
Treatment refractory	11	85
Prior methotrexate	13	100
Prior rituximab	12	92
Prior cranial radiation	4	31
Autologous Transplant	4	31
Disease sites		
CSF + Flow cytometry	9	50
Intraocular	3	11
Deep brain lesions	13	72
Peripheral Disease	3	11
Elevated LDH	10	56
IELSG risk groups		
0–1	3	17
2–3	7	39
4–5	8	44

Table 2

Toxicity

Toxicity and Groups	Grade 3 No (%)	Grade 4 No (%)	Grade 5 No (%)
Ibrutinib-Window Group Patients (n = 18)			
Non-Hematological			
Infection Pulmonary/CNS[1]			2 (11)
Hyponatremia	1 (6)		
DA-TEDDi-R Group Patients (n = 16)			
Hematological			
Neutropenia	10 (63)	15 (94)	
Thrombocytopenia	13 (81)	9 (56)	
Febrile Neutropenia	10 (69)		1 (6)
Non-Hematological			
Palmar-plantar erythrodysesthesia	2 (13)		
Mucositis	2 (13)	1 (6)	
Infection pulmonary[2]	8 (50)	1 (6)	
Infection other[3]	3 (19)		
Stroke			1 (6)
Ventricular arrhythmia			1 (6)
Intra-abdominal hemorrhage		1 (6)	
Nausea	1 (6)		
Diarrhea	2 (13)		

[1] Includes 2 patients with both pulmonary and CNS *Aspergillus*.

[2] Includes 5 patients with pulmonary *Aspergillus*.

[3] Includes 2 patients with CNS *Aspergillus*.

See also Table S1.

Table 3

Ibrutinib Pharmacokinetics

Patient Number	Plasma				CSF Ibrutinib PK				CSF penetration	Hours above IC_{50} (0.5 nM)	
	C_{max} (nM)	T_{max} (hr)	AUC_{0-24} (nM•hr)	$T_{½}$ (hr)	C_{max} (nM)	T_{max} (hr)	AUC_{0-24} (nM•hr)	AUC_{CSF}: AUC_{Plasma} (%)	AUC_{CSF}: AUC_{Plasma} Corrected (%)	Plasma	CSF
Dose 560 mg											
1	502	1	1343	10.2	1.99	2	10.1	0.75	27.9	24	4
2	145	2	565	4.6	0.69	2	2.7	0.48	17.8	24	2
3	77	2	412	3.1	1.28	2	6.55	1.6	58.9	24	4
4	72	1	434	2.6	1.54	4	17.6	4.1	148	24	8
5	162	2	691	8.5	2.0	2	12.4	1.8	66.3	24	10
6	99	1	429	6.3	0.71	2	2.51	0.58	21.6	24	4
Median	122	1.5	500	5.5	1.4	2	8.3	1.2	43.4	24	4
Range	75–502	1–2	412–1343	2.6–10.2	0.7–2	2–4	2.51–17.6	0.48–4.1	17.8–148	24	2–10
Dose 700mg											
7	581	1	2340	5.3	11.1	2	48.6	2.07	76.9	24	10
8	411	2	1880	2.4	1.63	2	12.2	0.65	24.1	10	10
9	164	2	968	3.8	0.69	4	10.9	1.12	41.6	24	3
10	577	2	1727	5.4	2.36	2	13.1	0.76	28.6	24	7
Median	494	2	1803	4.6	1.98	2	12.6	0.94	35.1	24	8.5
Range	164–581	1–2	968–2340	2.4–5.4	0.69–11.1	2–4	10.9–48.6	.65–2.07	24.1–76.9	10–24	3–10
Dose 840mg											
11	300	1	816	15.4	2.16	1	6.9	0.85	31.3	24	4
12	247	2	1213	4.1	1.66	4	10.2	0.84	31.2	24	7
13	426	2	1562	31.2	1.76	4	16.5	1.05	39.0	24	9
14	442	1	1343	23.3	2.68	2	8.5	0.63	23.4	24	4
15	144	4	1062	26.7	1.0	6	13.4	1.25	46.6	24	24
16	150	2	892	8.8	0.69	2	5.59	0.62	23.2	24	4
17	76	4	327	7.2	0.55	6	2.21	0.64	23.9	24	2

Patient Number	Plasma				CSF Ibrutinib PK				CSF penetration	Hours above IC_{50} (0.5 nM)	
	C_{max} (nM)	T_{max} (hr)	$AUC_{0–24}$ (nM•hr)	$T_{½}$ (hr)	C_{max} (nM)	T_{max} (hr)	$AUC_{0–24}$ (nM•hr)	$AUC_{CSF:}$ AUC_{Plasma} (%)	$AUC_{CSF:}$ AUC_{Plasma} Corrected (%)	Plasma	CSF
18	97	2	760	20.6	0.50	2	5.38	0.71	26.2	24	0
Median	199	2	977	18.1	1.33	3	7.7	0.78	28.7	24	4
Range	76–442	1–4	327–1562	4.1–31.2	0.50–2.68	1–6	2.21–16.5	0.62–1.25	23.2–46.6	24	0–24

See also Tables S2 and S3.